Hindawi
Mathematical Problems in Engineering
Volume 2024, Article ID 2834556, 15 pages
https://doi.org/10.1155/2024/2834556

Research Article

Numerical Simulation and Sensitivity Analysis Using RSM on Natural Convective Heat Exchanger Containing Hybrid Nanofluids

Saiful Islam,[1] **Md. Noor-A-Alam Siddiki**,[2] **and Md. Shahinur Islam**[2]

[1]*Department of Mathematics, Bangabandhu Sheikh Mujibur Rahman Science and Technology University, Gopalganj, Bangladesh*
[2]*Department of Computer Science and Engineering, Stamford University Bangladesh, Dhaka, Bangladesh*

Correspondence should be addressed to Saiful Islam; saiful.islam@bsmrstu.edu.bd

Received 18 September 2023; Revised 10 November 2023; Accepted 9 March 2024; Published 22 March 2024

Academic Editor: Babak Shotorban

This work presents a numerical analysis for exploring heat transfer phenomena in an enclosed cavity using magnetohydrodynamics natural convection. Because of the numerous real-world applications of nanofluids and hybrid nanofluids in industrial and thermal engineering developments, hybrid nanofluids are used as fluid mediums in the fluid field. A hexagonal-shaped heat exchanger is taken with two circular surfaces along the middle part. The upright circular surface acts as a homogeneous heat source, while the lower circular surface functions as a heat sink. The remaining portions of the adjacent walls are thermally insulated. The copper (Cu) and titanium dioxide (TiO_2) nanoparticles are suspended into water to make a hybrid nanofluid. For solving the corresponding governing equations, the weighted-residual finite element method is applied. To explain the major outcomes, isotherms, streamlines, and many others 2D and 3D contour plots are involved graphically with a physical explanation for different magnitudes of significant parameters: Rayleigh number ($10^3 \leq Ra \leq 10^6$), Hartmann number ($0 \leq Ha \leq 100$), and nanoparticle volume fraction ($0 \leq \phi \leq 0.06$). The novelty of this work is to apply response surface methodology on the natural convective hybrid nanofluid model, to visualize 2D and 3D effects, and to study the sensitivity of independent parameters on response function. Due to the outstanding thermal properties of the hybrid nanofluid, the addition of Cu and TiO_2 nanoparticles into H_2O develops the heat transfer rate to 35.85% rather than base fluid. Moreover, a larger magnitude of *Ra* and the accumulation of mixture nanoparticles result in the thermal actuation of a hybrid nanofluid. With greater magnetic impact, an opposite response is exhibited.

1. Introduction

Natural convective heat transfer has drawn consideration from a lot of today's researchers due to its plentiful straight industrial and technical uses in heat exchangers, house cooling and heating systems, nuclear reactors, solar collectors, electrical equipment, fire engineering, petrochemical industries, and so on. The key factors driving the attractiveness of the natural convective heat-transfer process are the easy and truncated price of building geometrical domains, even if forced and natural convection are primarily two methods of convection for heat transfer in a fluid medium. Natural convection has typically happened because of the temperature variance and the buoyancy forces. Due to the simplicity and vast applications of natural convection heat transfer, at different times, frequent studies have previously been done [1–6]. To increase the efficiency of heat transmission in both natural and force convective thermal engineering processes, nowadays, nanofluid is imposed with common fluid into the fluid domain. Actually, nanofluid is a comparatively new class of thermal engineering fluid combined by suspending nanoparticles (size smaller than 100 nm), such as Cu, Ag, Al_2O_3, or TiO_2, in common liquids. These common liquids (for instance, engine oil, water, pump oil, ethanol, etc.) are known as base fluids. First, Choi and Eastman [7] introduced nanofluid at Argonne National Laboratory, USA, in 1995. Nanofluid has numerous practical applications in industry and health science, such as in semiconductors, solar engineering, thermal storage systems, microelectronics, electronic devices, computer processors, nuclear reactor cooling, biomedical engineering, cancer

therapy, etc. To heighten the thermal performance of base fluid, at different times, already there have been extensive studies about Cu, CuO, Ag, Al_2O_3, Fe_3O_4, and TiO_2 suspension into a base fluid in numerous fluid domains [8–16]. To explain the significance of nanofluid, Rostami et al. [17] described natural convective heat transfer models with and without the existence of nanoparticles into the base fluids. Ellahi et al. [18] investigated carbon nanotubes (CNTs)-H_2O nanofluid-based heat transfer performance. Park et al. [19] explored free convection as impacted by a temperature variation between a heated interior cylinder and a cold external slanted square hollow. Waqas et al. [20] explored natural convective heat transfer in a horizontal annulus with a fin using Cu–H_2O nanofluid. They arrived at the conclusion that raising the value of ϕ lowered the velocity field while raising the value of ϕ and Ra increased the thermal performance.

Furthermore, to get better heat transfer performance nowadays, two different nanoparticles are intermixed into a base fluid, and this suspension is known as a hybrid nanofluid. By choosing the materials of nanoparticles accurately, they would play a significant essence of each other. Actually, a single-component nanofluid does not have all the desirable characteristics needed for a given application. For example, metal oxide nanoparticles (CuO, MgO, TiO_2, Al_2O_3, etc.) have lower heat conductivity and greater chemical stability. On the contrary, nanoparticles that are metallic (Cu, Al, Ag, Au, etc.,) are very reactive and unstable, and they also have good thermal conductivity. As a result, by combining these two types of nanoparticles, improved physical and chemical properties can achieve while also improving the host fluid's capacity for heat transfer. Due to its synergism, hybrid nanofluid exhibits higher thermal conductivity than traditional nanofluids. Recently, numerous researchers have done both numerically and experimentally to study the novel technological concept of hybrid nanofluids [21–26]. Chamkha et al. [27] studied how well a hybrid nanofluid transferred heat over time in a semicircular chamber. Khadim et al. [28] analyzed Cu–Al_2O_3–H_2O nanofluid in a porous enclosure, making a wavy surface where the bottom surface was taken as a heat source. Biswas et al. [29] explored natural convective magnetohydrodynamics (MHD) nanofluid by taking Cu and Al_2O_3 into water in a porous oblique wavy vertical wall enclosure that was heated. In another work, Rashad et al. [30] analyzed again the consequences of Cu–Al_2O_3–H_2O nanofluid enclosed in a triangle with a uniform magnetic and thermal field. The simulation was resolved by employing the finite difference technique, where results showed a significant effect for increasing the nanoparticle volume fraction. Takabi and Salehi [31] explained natural convective establishment in a corrugated cavity with a nonuniform heat lowermost wall occupied with an Al_2O_3–Cu–H_2O mixture. Devi and Devi [32] modeled a 3D boundary layer hybrid nanofluid flow across an extending sheet using Newtonian heating and Lorentz force.

Furthermore, the scientific discipline known as MHD is responsible for describing how magnetic force affected an electrically conducting liquid. MHD is predisposed by a variety of factors, including the radiation in X-rays, the magnetic field on earth, cooling of fission reactors, solar wind, therapy for tumor treatment, etc. Due to these practical applications, many researchers examined MHD heat transport in a number of distinct geometries over time [33–37]. Sheikholeslami et al. [38] analyzed natural convection with thermal radiation impact using Al_2O_3–water in a closed cavity. Prakash et al. [39] did another numerical analysis on MHD natural convection in a partially ventilated curved permeable aperture containing a nanofluid. They came to the conclusion that as the Hartmann number developed, the overall convection decreased. Mourad et al. [40] also explored natural convective MHD using Fe_3O_4–MWCNT–water nanofluid in a porous cavity with consistent magnetic field, where entropy generation was calculated. Over a porous sheet, Mahesh et al. [41] completed a different investigation on MHD hybrid nanofluid to investigate the impacts of radiation. Ahmed et al. [42] explored the consequences of employing hybrid nanofluid on MHD radiative natural convection in porous configurations.

From the aforementioned review of the literature, it is apparent that the MHD natural convection has a great interest to researchers since it has revolutionary implications, across a wide range of engineering fields. Despite several studies on various closed cavities were carried out over time to explore the behavior of the MHD natural convective heat transfer process, only a few studies were carried out on hexagonal enclosures using different nanoparticles in more recent years [43–46]. Again, relatively little research on heat exchangers, mechanical devices that transport heat between two or more liquids, was done in order to develop a quick heat transfer system [47–49]. Moreover, to visualize the 2D and 3D effects of response function and study the sensitivity analysis of independent factors, the response surface methodology (RSM) is involved in this natural convective hexagonal-shaped heat exchanger that contains a hybrid nanofluid. That is, we investigate the sensitivity analysis of the natural convective heat transfer procedure for a hexagonal heat exchanger loaded with Cu–TiO_2–H_2O hybrid nanofluid considering the direct implication of magnetic field. According to the highest level of the writers' knowledge, no research has yet been done on this issue. The regulatory equations are simulated using a form of computation known as the finite element method (FEM) [50]. So, the leading purpose of this simulation is to investigate natural convection in a closed cavity covered with hybrid nanofluid statistically and numerically and examine how much the overall heat transfer rate is exaggerated by the Ra, Ha, and ϕ. This numerical investigation is designed to provide responses to the subsequent research questions. Such as:

(i) What is the behavior of fluid flow and heat transfer rate on this heat exchanger?
(ii) What is the importance of adding nanofluid and hybrid nanoparticles into base fluid?
(iii) What is the best-fitted correlation between the response function and independent factors?
(iv) How much response function is sensitive for the independent factors?

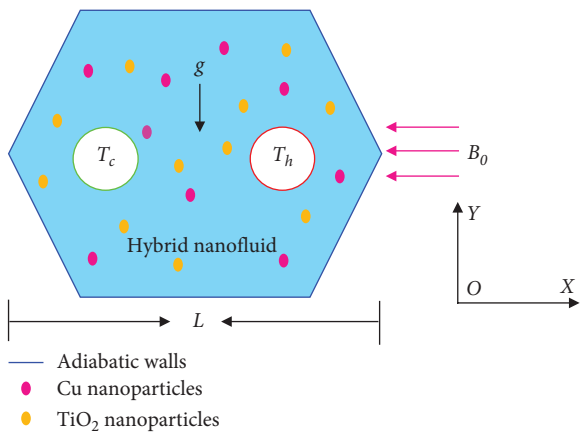

FIGURE 1: Schematic view of the proposed hexagonal model.

2. Mathematical and Physical Model

In this work, a hexagonal-shaped heat exchanger is chosen as a fluid domain that is covered by TiO_2 and Cu solid nanoparticles into water (H_2O). This fluid is steady, Newtonian, and incompressible that has a direct bearing on the magnetic field. The horizontal length of this cavity is L. Two cylindrical pipes, diameter $0.10\,L$, are taken into the cavity along the middle part of the cavity, where the right side has a uniform heat source (T_h) and the left one acted as a heat sink (T_c). A physical diagram of this proposed hybrid nanofluid model is characterized in Figure 1. However, all of the bordering walls remain insulated, and the gravitational force due to acceleration (g) is acted downward. Moreover, a uniform magnetic field (B_0) is acted from the right to left. The shape of the Cu and TiO_2 nanoparticles are estimated alike in shape and size, and all outer walls are considered as no-slip. The taken thermo-physical appearances of base fluid and solid particles are described in Table 1.

2.1. Governing Equations. To formulate this MHD 2D heat exchanger using hybrid nanofluid, the involved governing equations are continuity, momentum, and energy equations that are termed as follows [13]:

$$\nabla.\,\overline{v} = 0, \tag{1}$$

$$\rho_{\text{hnf}}(\overline{v}.\nabla)\overline{v} = -\nabla p + \mu_{\text{hnf}}(\nabla^2\overline{v}) + F, \tag{2}$$

$$(\rho c_p)_{\text{hnf}}(\overline{v}.\nabla T) = \kappa_{\text{hnf}}(\nabla^2\ T), \tag{3}$$

where the velocity field $\overline{v} = (u, v)$ acted along X and Y axes, respectively. The buoyancy forces and the external magnetic field are treated as body forces (F) acting across the Y-axis in the momentum equation. As a consequence, $F = g(\rho\beta)_{\text{hnf}}\,(T - T_c) - \sigma_{\text{hnf}}\,B_0^2 v$ is substituted in Y-momentum equation. The corresponding boundary conditions are defined as follows:

$$\left.\begin{aligned} u = 0, v = 0, T = T_c &\ \text{ on left circular edge} \\ u = 0, v = 0, T = T_h &\ \text{ on right circular edge} \\ \text{and}\ \ u = v = 0, \frac{\partial T}{\partial n} = 0 &\ \text{ on others boundaries} \end{aligned}\right\}, \tag{4}$$

where n is the perpendicular vector acted on the heated surface.

2.2. Nanofluid's Properties. The thermo-physical belongings of base fluid and nanoparticles are prearranged earlier. Actually, the belongings of nanofluid lie on base fluid and nanoparticle's characteristics. So, to compute the hybrid nanofluid belongings, the associations described in Table 2 are involved.

2.3. Dimensionless Mathematical Model. The subsequent dimensionless quantities [44] are taken to make dimension-free equations for governing Equations (1)–(3): $X = \frac{x}{L}$, $Y = \frac{y}{L}$, $U = \frac{uL}{\alpha_{bf}}$, $V = \frac{vL}{\alpha_{bf}}$, $P = \frac{pL^2}{\rho_{bf}\alpha_{bf}^2}$ and $\theta = \frac{T-T_c}{T_h-T_c}$. Employing the abovementioned dimensionless variables listed above, Equations (1)–(3) turn into the following:

$$\frac{\partial U}{\partial X} + \frac{\partial V}{\partial Y} = 0, \tag{5}$$

$$U\frac{\partial U}{\partial X} + V\frac{\partial U}{\partial Y} = -\left(\frac{\rho_{bf}}{\rho_{\text{hnf}}}\right)\frac{\partial P}{\partial X} + \left(\frac{\mu_{\text{hnf}}}{\mu_{bf}}.\frac{\rho_{bf}}{\rho_{\text{hnf}}}\right)Pr\,(\nabla^2 U), \tag{6}$$

$$\begin{aligned} U\frac{\partial V}{\partial X} + V\frac{\partial V}{\partial Y} = &-\left(\frac{\rho_{bf}}{\rho_{\text{hnf}}}\right)\frac{\partial P}{\partial Y} + \left(\frac{\mu_{\text{hnf}}}{\mu_{bf}}.\frac{\rho_{bf}}{\rho_{\text{hnf}}}\right)Pr\,(\nabla^2 V) \\ &+ \frac{(\rho\beta)_{\text{hnf}}}{\rho_{\text{hnf}}\beta_{bf}}Ra\,Pr\,\theta - \left(\frac{\rho_{bf}}{\rho_{\text{hnf}}}.\frac{\sigma_{\text{hnf}}}{\sigma_{bf}}\right)Pr\,Ha^2 V, \end{aligned} \tag{7}$$

$$U\frac{\partial \theta}{\partial X} + V\frac{\partial \theta}{\partial Y} = \left(\frac{\alpha_{\text{hnf}}}{\alpha_{bf}}\right)\nabla^2\theta, \tag{8}$$

where Rayleigh number (Ra), Prandtl number (Pr), and Hartmann number (Ha) are three significant parameters generated from the above equation, which are defined, respectively, as: $Ra = \frac{g\beta_{bf}(T_h-T_c)L^3}{\upsilon_{bf}\alpha_{bf}}$, $Pr = \frac{\upsilon_{bf}}{\alpha_{bf}}$, and $Ha = B_0 L\sqrt{\frac{\sigma_{bf}}{\mu_{bf}}}$. Moreover, the dimension-free boundary conditions reformed as follows:

$$\left.\begin{aligned} U = V = 0, \theta = 0 &\ \text{ on left circular edge} \\ U = V = 0, \theta = 1 &\ \text{ on right circular edge} \\ \text{and}\ \ U = V = 0, \frac{\partial \theta}{\partial N} = 0 &\ \text{ on other walls} \end{aligned}\right\}. \tag{9}$$

Furthermore, the average heat transfer rate from the surface that was heated is determined by the following:

Table 1: Thermo-physical individual of base fluid and solid particles [16, 24].

Base fluid and nanoparticle	c_p (J.kg^{-1}.K^{-1})	ρ (kg.m^{-3})	κ (W.m^{-1}.K^{-1})	β (K^{-1})	σ (Sm^{-1})	μ (kg.m^{-1}.s^{-1})	Pr
H_2O	4,179	997.1	0.613	21×10^{-5}	0.05	8.91×10^{-4}	6.9
TiO_2	686.2	4,250	8.953	0.9×10^{-5}	3.5×10^{6}	—	—
Cu	385	8,933	401	1.67×10^{-5}	5.96×10^{7}	—	—

Table 2: Thermo-physical belongings of hybrid nanoparticles.

Hybrid nanofluid's properties		Applied correlations
Concentration of nanoparticles	:	$\phi=\phi_{\mathrm{Cu}}+\phi_{\mathrm{TiO_2}}$
Density of nanofluid	:	$\rho_{\mathrm{hnf}}=(1-\phi)\rho_{bf}+\phi\,\rho_{sp}$ where $\phi\rho_{sp}=\phi_{\mathrm{Cu}}\rho_{\mathrm{Cu}}+\phi_{\mathrm{TiO_2}}\rho_{\mathrm{TiO_2}}$
Specific heat capacity	:	$(\rho c_p)_{\mathrm{hnf}}=(1-\phi)(\rho c_p)_{bf}+\phi(\rho c_p)_{sp}$ where $\phi(\rho c_p)_{sp}=\phi_{\mathrm{Cu}}(\rho c_p)_{\mathrm{Cu}}+\phi_{\mathrm{TiO_2}}(\rho c_p)_{\mathrm{TiO_2}}$
Thermal conductivity	:	$k_{\mathrm{hnf}}=k_{bf}\left\{\frac{k_{sp}+2k_{bf}-2\phi(k_{bf}-k_{sp})}{k_{sp}+2k_{bf}+\phi(k_{bf}-k_{sp})}\right\}$ where $\phi k_{sp}=\phi_{\mathrm{Cu}}k_{\mathrm{Cu}}+\phi_{\mathrm{TiO_2}}k_{\mathrm{TiO_2}}$
Thermal diffusivity	:	$\alpha_{\mathrm{hnf}}=\frac{\kappa_{\mathrm{hnf}}}{(\rho c_p)_{\mathrm{hnf}}}$
Dynamic viscosity	:	$\mu_{\mathrm{hnf}}=\mu_{bf}(1+2.5\phi+6.5\phi^2)$
Thermal expansion coefficient	:	$(\rho\beta)_{\mathrm{hnf}}=(1-\phi)(\rho\beta)_{bf}+\phi(\rho\beta)_{sp}$ where $\phi(\rho\beta)_{sp}=\phi_{\mathrm{Cu}}(\rho\beta)_{\mathrm{Cu}}+\phi_{\mathrm{TiO_2}}(\rho\beta)_{\mathrm{TiO_2}}$
Electrical conductivity	:	$\sigma_{\mathrm{hnf}}=\sigma_{bf}\left[1+\frac{3\phi(\frac{\sigma_{sp}}{\sigma_{bf}}-1)}{(\frac{\sigma_{sp}}{\sigma_{bf}}+2)-\phi(\frac{\sigma_{sp}}{\sigma_{bf}}-1)}\right]$ where $\phi\sigma_{sp}=\phi_{\mathrm{Cu}}\sigma_{\mathrm{Cu}}+\phi_{\mathrm{TiO_2}}\sigma_{\mathrm{TiO_2}}$

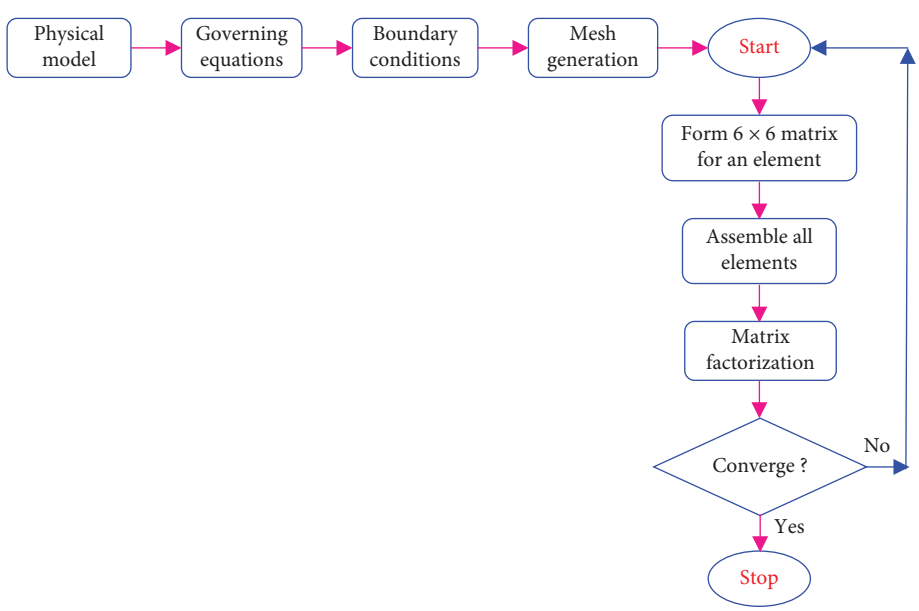

Figure 2: A comprehensive flowchart of the computing technique.

$$\mathrm{Nu}_{\mathrm{av}}=-\left(\frac{k_{\mathrm{hnf}}}{k_{bf}}\right)\int_{\mathrm{HS}}\frac{\partial\theta}{\partial N}dS, \tag{10}$$

where N is the perpendicular vector that acts on the heated surface. Additionally, the stream function ψ is defined as: $U=\frac{\partial\psi}{\partial Y}$, $V=-\frac{\partial\psi}{\partial X}$. Here, the plus sign signifies the anticlockwise

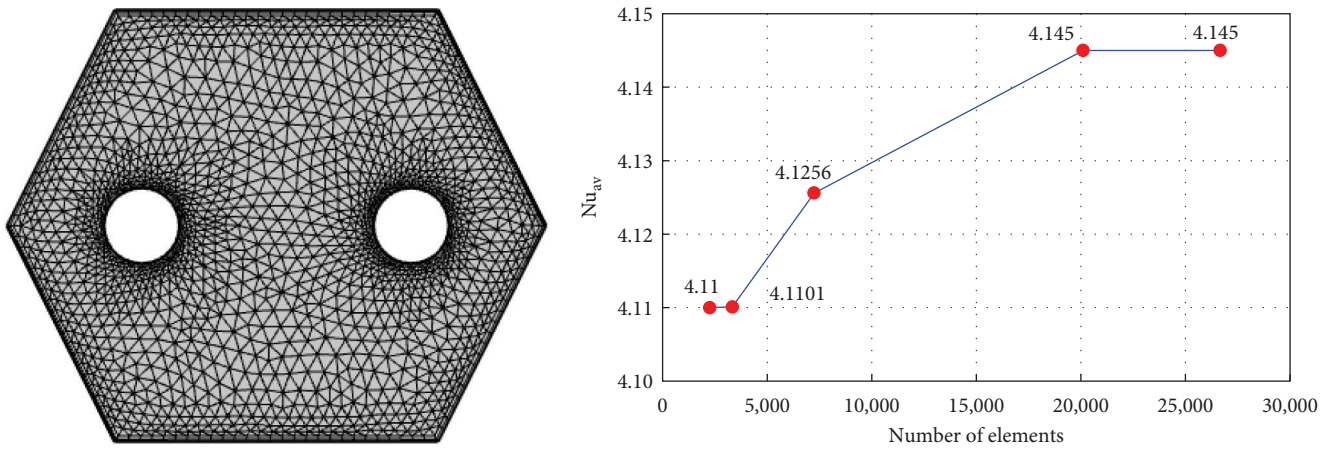

(a) (b)

Figure 3: (a) Type of meshing entire domain and (b) the grid test by Nu_{av}.

circulation, while the minus sign implies the clockwise circulation of streamlines. Moreover, $\frac{\partial^2\psi}{\partial X^2}+\frac{\partial^2\psi}{\partial Y^2}=-\left(\frac{\partial V}{\partial X}-\frac{\partial U}{\partial Y}\right)=-\Omega$ is the equation of vorticity, and the vorticity vector is Ω.

3. Numerical Analysis

3.1. Solution Methodology. For this hybrid nanofluid-based hexagonal heat exchanger model, the dimensionless governing Equations (5)–(8) are simulated by utilizing the Galerkin weighted residual FEM. The entire domain is split into distinct triangular form elements for calculating velocity and temperature, taking into account a quadratic interpolation function. Alternatively, the linear interpolation procedure is also engaged to compute the pressure gradient. The Newton–Raphson iteration procedure using MATLAB programing is employed to construct a group of nonlinear algebraic equations to formulate those governing equations. For this approach, the criteria for convergence is derived for all variables that are unable to have a significant impact in the sense that $|\Pi^{i+1}-\Pi^{i}|<\delta=10^{-5}$ where $\Pi(U,V,\theta)$ represents the value of the iteration, and $i+1$ and i are two sequential steps describes the whole procedure. A complete process for this FEM was elaborately described in [48]. A comprehensive flowchart is described in Figure 2.

3.2. Grid Sensitivity Analysis. To obtain the most elements possible using this finite element technique, a grid test is explained by taking the corresponding parameters: $Ra=10^4$, $\phi=0.02$, and $Ha=10$. Also, $Pr=6.9$ is considered for base fluid. Furthermore, to implement this sensitivity test for making proper meshing, the optimal value of the Nu_{av} is chosen. This fluid model's entire domain has been divided into five separate numbers (2,256, 3,338, 7,250, 20,110, and 26,662) of triangular-shaped elements. Figure 3(a) represents a sample of triangular-type meshing. Also, Table 3 and Figure 3(b) show the calculated values of Nu_{av} for various numbers of triangle elements in this fluid domain. It is obvious that the value of Nu_{av} for the 20,110 number of elements is virtually identical to the value found for the next larger number of components. As a result, the 20,110 triangular components are recommended for meshing and completing this fluid model.

Table 3: Numerical values of Nu_{av} for different elements.

Elements	2,256	3,338	7,250	20,110	26,662
Nu_{av}	4.110	4.1101	4.1256	4.1450	4.1450

3.3. Code Validation. The scientific reliability of this simulation is tested utilizing streamline and isotherm contours using Park et al. [19], where $Ra=10^3$ and $Pr=0.7$ are used. Also, the length of the square cavity was one, and the inner circle was 0.2 that is represented in Figure 4. The outermost sides served as heat sinks, while the inner circular surface in the center served as a uniform heat source. The streamline and isotherm contours are very alike to the current result. The Nu_{av} is also compared, in Table 4, to the results of Park et al. [19], which reveal a similar consequence. That is, these results demonstrate good agreement with the present study, which increases trust in the current analysis.

4. Results and Discussion

The achieved outcomes are reported using streamlines, isotherms, and Nu_{av} to investigate this hexagonal natural convective fluid model by using a hybrid nanofluid. The influence of *Ra, Ha*, and ϕ are illustrated with physical interpretation using $Ra=10^4$, $Pr=6.9$, $Ha=10$, and $\phi=0.02$ as standards. The importance of adding different nanoparticles into a base fluid is explained graphically. Moreover, a sensitivity analysis is conducted to demonstrate how *Ra, Ha*, and ϕ impact the Nu_{av} by involving another statistical method called RSM. This numerical simulation on a natural convective hexagonal heat exchanger can predict a best-fitted regression equation for independent factor and response function. Also, the importance of adding hybrid nanoparticles into base fluid can be explained with 2D and 3D visualization for response function.

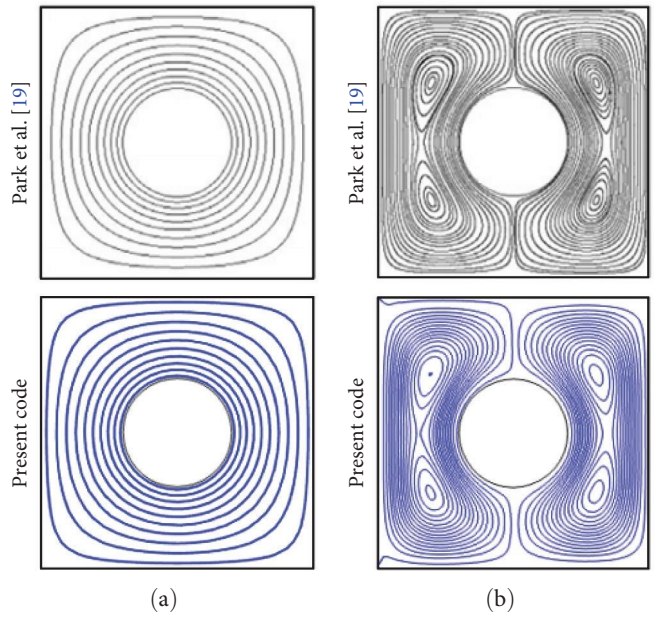

Figure 4: Comparison between obtained result and Park et al. [19]: (a) isotherms and (b) streamlines.

Table 4: Numerical values of Nu_{av} with Park et al. [19].

Parameter (Ra)	10^3	10^4	10^5	10^6
Nu_{av}	5.024	5.129	7.817	14.298
Present study	5.023	5.132	7.816	14.296

4.1. Influence of Rayleigh Number. Here, Figure 5 illustrates streamline and isotherm contours that reveal the impact of Ra from 10^3 to 10^6 on fluid motion and heat transfer when $Ha = 10$, $Pr = 6.9$, and $\phi = 0.02$ are keeping fixed. Here, Figure 5(a) displays the control of Ra on streamlines, showing that at a low value of Ra, the streamlines are almost perfectly uniform (dumbbell) along the vertical mid-point of the cavity. It is clearly observed that when the Ra shifted from 10^3 to 10^5, the pattern of the streamline is almost the same, but the velocity field increased sufficiently. But at the higher Ra (10^6), the streamlining pattern varies dramatically. The convective mode of heat transfers around the right hot cylinder gradually became stronger due to a significantly higher buoyancy effect. The streamlines have now extended out from the right hot cylinder to the left one. Once more, fluid from the nearby left cylinder that is considerably colder flows into the hot right cylinder. As a result, two small vortices inside the main vortex and the other two rotating rolls on both sides of the hot cylinder and cool cylinder are generated. These vortices show that enormous convection occurs at high Ra values.

On the other hand, the isotherm contours demonstrate the temperature transmission mode (conduction or convection) as well as the practical benefits of temperature. Figure 5(b) illustrates how Rayleigh's number affects the contours of the isotherm. It is evident that convection is less within the cavity when the Ra is low (10^3), as evidenced by the fact that the isotherm contours are practically parallel along the vertical axis at the central part of the cavity. The cavity center's low isotherm compactness indicates weakly convective temperature flow. With rising Ra, the isotherm contours become excessively deformed and begin to flatten from hot to cool cylinders. Moreover, at high Ra (10^6), they almost completely flatten. The real cause of this is an increase in fluid velocity driven by a rise in Ra. As a consequence, the naturally occurring convective heat transmission from the right's hot circular exterior to the left cooler circular exterior. At low Ra (10^3–10^5) value, the rate of heat transmission is relatively smaller but at higher Ra (10^6) value, the change of heat is very significant.

4.2. Effect of Hartmann Number. Figure 6 illustrates the effect of Ha, which indicates the influence of the magnetic field, using isotherms and streamlines for keeping $\phi = 0.02$, $Pr = 6.9$, and $Ra = 10^4$. The fluctuation of streamlines for diverse values of Ha is depicted in Figure 6(a).

For each value of the Ha taken into consideration, the figures display a comparable symmetric pattern (dumbbell) along a vertical line at the center of the streamlines. It is also clearly detected that at $Ha = 0$, in nonattendance of the external magnetic field, the streamlines are at maximum state.

However, with the development of Ha (25, 50, and 100), that means when an exterior magnetic field is acted on the system, the streamlines gradually disappear, which indicates that flow strength drops with a growing magnetic field. The physical significance of this consequence is that when an exterior magnetic field is pragmatic, a greater field interacts with moving fluid, which possesses magnetic impressionability and reduces flow movement inside the cavity. Additionally, the Lorentz force produced by put on a magnetic field has the tendency to resist the fluid movement, which weakens the streamlines inside the cavity. Additionally, the isothermal lines in Figure 6(b) suggest that there is a change, but it is not very noticeable for larger Ha (50 and 100). This has a

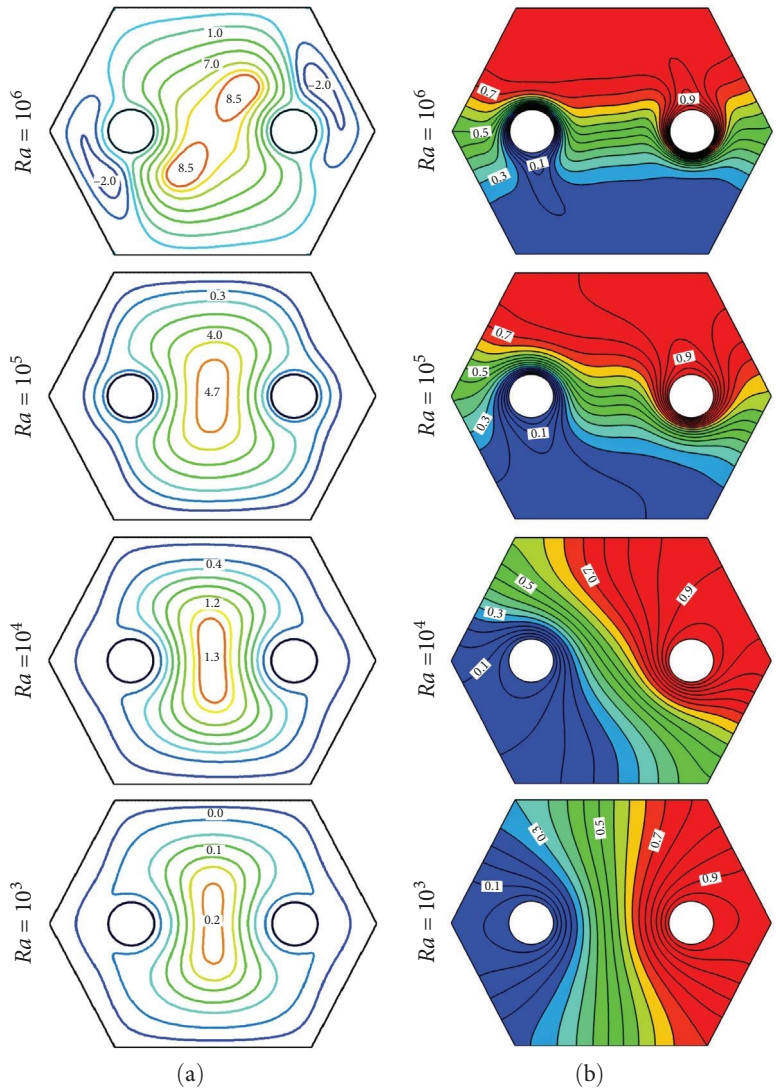

Figure 5: Effect of *Ra* on (a) streamlines and (b) isotherms.

physical meaning in that fluid movement is restricted by the acted magnetic field. Thus, the isothermal lines change a very little, as is seen from Figure 6(b), and the heat convection caused by fluid movement is minimal.

4.3. Effect of Hybrid Nanofluid. The Nu_{av} is employed with varying values of *Ra* and *Ha* to describe and display the heat transfer rate for various types of fluids such as base fluid, Cu–H_2O, TiO_2–H_2O, and Cu–TiO_2–H_2O. For changing the value of *Ra*, the Nu_{av} growths gradually for pure fluid (H_2O), TiO_2–H_2O nanofluid, Cu–H_2O nanofluid, and hybrid nanofluid (Cu–TiO_2–H_2O), which is depicted by Figure 7(a). When TiO_2 nanoparticles are added into water, the heat transfer rate is rapidly developed rather than the pure base fluid. Again, if Cu nanoparticles are added into the water, then the heat transfer rate is also developed rather than the pure base fluid.

Moreover, if hybrid nanoparticles are added into the base fluid, the Nu_{av} is developed remarkably. This time, the Nu_{av} is the greatest than the mono-nanofluid or only base fluid. Furthermore, Figure 7(b) shows an enhancement of Nu_{av} with adding off mono-nanoparticles or hybrid nanoparticles. The results show that the Nu_{av} of Cu–TiO_2–H_2O hybrid nanofluid is more sophisticated than the Cu–H_2O nanofluids, though the rate of Nu_{av} reduces with rising *Ha* factor for all types of fluid combination. That is, Figure 7 shows that the Cu–TiO_2–H_2O hybrid nanofluid has superior heat transport ability than TiO_2–H_2O nanofluid or Cu–H_2O nanofluid because of its outstanding thermal properties. This is one of the primary motives for involving hybrid nanofluid instead of base fluid or mono-nanofluid.

4.4. RSM. The statistical technique RSM is used to analyze the impact of response function (Nu_{av}) caused by the relevant factors (*Ra, Ha*, and ϕ). RSM provides one of the most successful approaches for modeling multidimensional situations in which the input factors influence the interest-generating responses simultaneously [51]. Though other RSM algorithms exist, the second-order (quadratic) RSM approach generally proves adequate for approximating the response. First, a quadratic-type RSM model can be considered as follows:

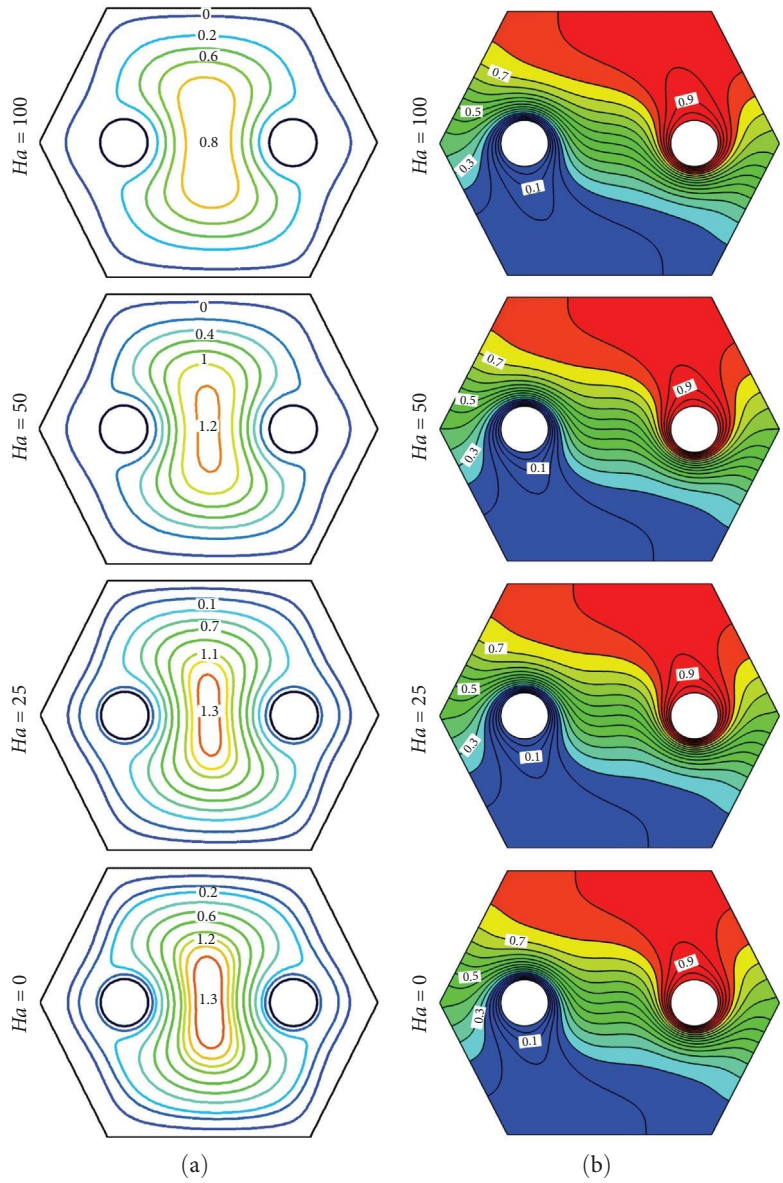

FIGURE 6: Effect of Ha on (a) streamlines and (b) isotherms.

$$y = d_0 + \sum_{i=1}^{3} d_i x_i + \sum_{i=1}^{3} d_{ii} x_i^2 + \sum_{i=1}^{3} d_{ij} x_i x_j, \tag{11}$$

where y, d_0, d_i, and d_{ii} denote the response function, terms of intercept, coefficient of linear and quadratic term of ith factor, respectively. Also, d_{ij} expresses the coefficient of interacting term of ith and jth factors. Furthermore, the factors Ra, Ha, and ϕ are used as input factors, while $\mathrm{Nu}_{\mathrm{av}}$ is occupied as response term (y). The foremost aim of this RSM is to find the best-fitted connection among independent factors related to this proposed heat exchanger model and response function. The central composite design (CCD) based second-order RSM is involved due to the perfectness of the second-order regression model in both experimental and numerical simulation-type datasets [52]. Here, $0 \le \phi \le 0.06$, $10^3 \le Ra \le 10^6$, and $0 \le Ha \le 100$ are considered the lower and upper limits of independent factors. This algorithm takes in a total of 20 runs, 8 cubes, 6 centers, and 6 axial points for 3 independent factors.

In Table 5, the codded levels for input factors of this CCD-based RSM model are described. Also, Table 6 expresses the values of the response function, received from FEM calculation, for different runs. Furthermore, Table 7 shows the results for this RSM-based simulation, where the quantity DOF (degrees of freedom) specifies the maximum number of stand-alone terms. Also, the score of the sum of squares (SS) is quite satisfactory. Furthermore, the p-value, the probability value for null hypothesis becoming true, is a critical indicator of this statistical research. Since a small p-value implies that the null hypothesis is rejected, a very small p-value (generally less than 5%) recommends the model is statistically significant for the

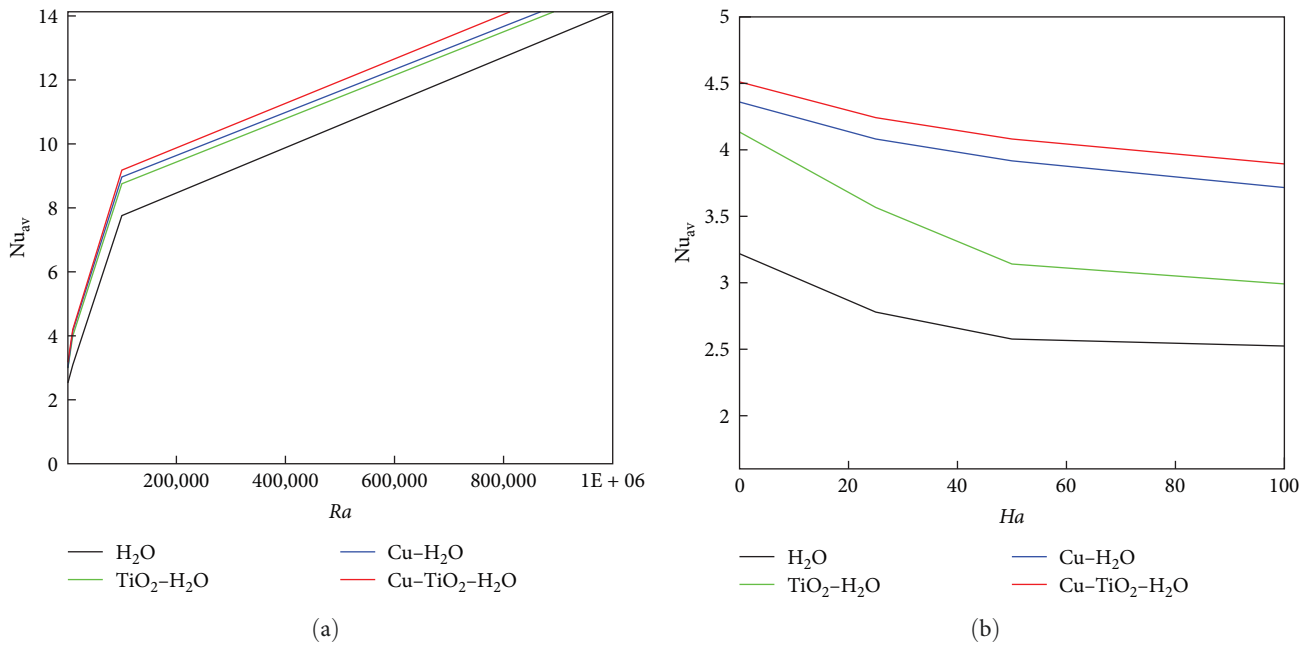

Figure 7: Comparison of thermal enactment by Nu_{av} for (a) *Ra* and (b) *Ha*.

Table 5: Codded levels for input factors.

Factors	Level		
	−1 (lowest)	0 (medium)	1 (highest)
Ra	10^3	500,500	10^6
Ha	0	50	100
ϕ	0	0.03	0.06

Table 6: Levels of input factors and response function.

Run order	Coded values			Real values			Response
	A: *Ra*	B: Ha	C: ϕ	*Ra*	*Ha*	ϕ	Nu_{av}
1	0	0	0	500,500	50	0.03	12.854
2	−1	0	0	1,000	50	0.03	2.9985
3	0	1	0	500,500	100	0.03	12.063
4	−1	1	1	1,000	100	0.06	3.5373
5	0	−1	0	500,500	0	0.03	13.159
6	0	0	1	500,500	50	0.06	13.473
7	0	0	0	500,500	50	0.03	12.854
8	1	1	−1	1,000,000	100	0	8.3363
9	−1	−1	−1	1,000	0	0	2.5269
10	0	0	0	500,500	50	0.03	12.854
11	−1	−1	1	1,000	0	0.06	3.5396
12	0	0	0	500,500	50	0.03	12.854
13	1	−1	1	1,000,000	0	0.06	16.695
14	0	0	−1	500,500	50	0	9.2798
15	−1	1	−1	1,000	100	0	2.5174
16	0	0	0	500,500	50	0.03	12.854
17	1	−1	−1	1,000,000	0	0	14.285
18	1	0	0	1,000,000	50	0.03	15.216
19	0	0	0	500,500	50	0.03	12.854
20	1	1	1	1,000,000	100	0.06	14.689

Table 7: ANOVA for Nu_{av} using RSM.

Source	DOF	SS	*F*-value	*p*-Value	Comment
Model	9	426.03	100.56	<0.0001	Significant
Ra	1	292.70	621.77	<0.0001	—
Ha	1	8.21	17.45	0.0019	—
ϕ	1	22.47	47.72	<0.0001	—
Ra^2	1	32.30	68.61	<0.0001	—
Ha^2	1	0.0162	0.0344	**0.8566**	—
ϕ^2	1	3.69	7.83	0.0188	—
Ra.Ha	1	7.89	16.75	0.0022	—
Ra.ϕ	1	5.66	12.03	0.0060	—
Ha.ϕ	1	1.95	4.14	**0.0691**	—
Lack-of-fit	5	4.71	—	—	Insignificant
Pure error	5	0.000	—	—	—

Note. $R^2 = 98.91\%$, adjusted $R^2 = 97.92\%$. Values indicated in the bold font denote insignificant terms ($p > 0.05$).

dataset given from numerical simulation. The adjusted R^2 value is 98.91% that demonstrate the framework is appropriate for conniving the Nu_{av}. Another key statistic that needs to be extremely low for a model to be judged appropriate is the lack-of-fit. Equation (12) expresses a general quadratic RSM model for investigating the association among the parameters *Ra*, *Ha*, ϕ, and the Nu_{av}.

$$y = d_0 + d_1 Ra + d_2 Ha + d_3 \phi + d_{11} Ra^2 + d_{22} Ha^2 + d_{33} \phi^2 + d_{12} Ra.Ha + d_{13} Ra.\phi + d_{23} Ha.\phi, \tag{12}$$

where $d_0, d_1, d_2, d_3, d_{11}, d_{22}, d_{33}, d_{12}, d_{13}$, and d_{23} represents the coefficients of the above regression line.

Table 8: Regression coefficients for Nu_{av} that are predicted based on RSM.

Coefficients	d_0	d_1	d_2	d_3	d_{11}	d_{22}	d_{33}	d_{12}	d_{13}	d_{23}
Values	12.73	5.41	−0.9062	1.50	−3.43	0.0767	−1.16	−0.9929	0.8413	0.4937
p-values	—	<0.0001	0.0019	<0.0001	<0.0001	**0.8566**	0.0188	0.0022	0.0060	**0.0691**

Values indicated in the bold font denote insignificant terms ($p > 0.05$).

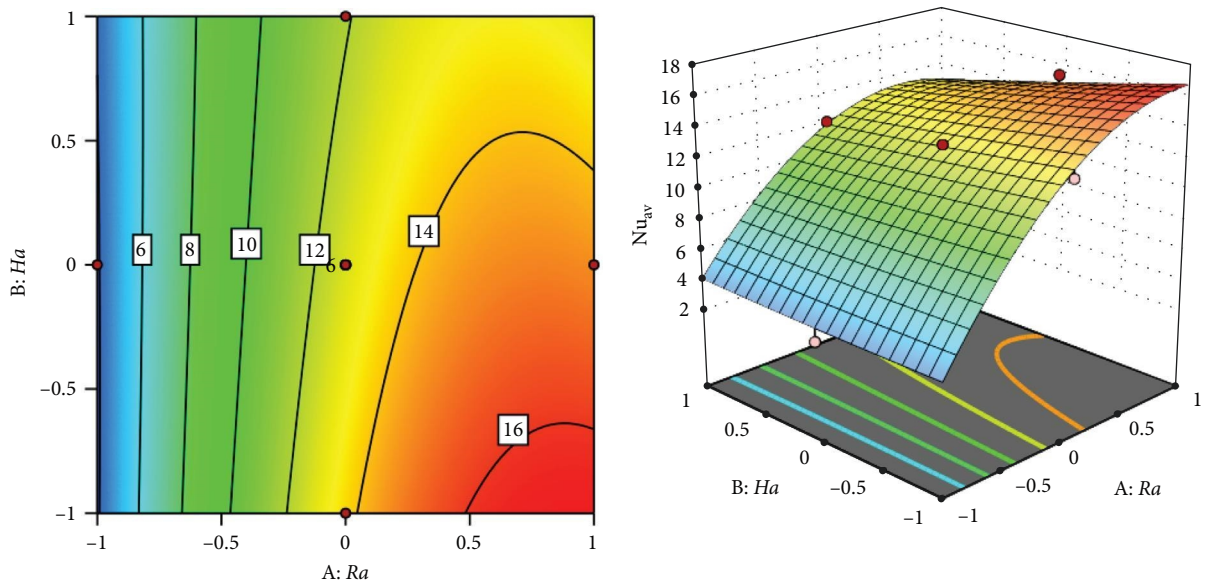

(a) (b)

Figure 8: Effect on Nu_{av} for Ra and Ha: (a) 2D sight and (b) 3D sight.

Table 8 also shows the estimated coefficients of Equation (12) for Nu_{av} with the corresponding p-value. Because of the significance of the p-value, only significant terms based on p-values are employed to build an acceptable regression equation. Nonsignificant terms have been ignored (bold emphasized).

That is, the terms Ha^2 and $Ha.\phi$ are completely unimportant for the regression Equation (12) of Nu_{av}. As a result, the connection between Nu_{av} and the input factors can be mathematically described as follows:

$$Nu_{av} = 12.73 + 5.41Ra - 0.9061Ha + 1.50\phi - 3.43\ Ra^2 - 1.16\phi^2 - 0.9929Ra.Ha + 0.8413Ra.\phi \quad (13)$$

4.5. Analysis of Response Surface. In this part, Figures 8–10 show two and 3D plots of the response surface derived with RSM to investigate the influence of independent factors on Nu_{av}. The impact of Ra and Ha on Nu_{av} is seen in Figure 8(a). This 2D contour map makes it evident that as Ra enlarged but Ha lessened, the response function increased. In a definite value of the magnetic field, the value of the Nu_{av} is developed while ϕ remains constant. For example, when the value of Ra is raised to 500,500 (codded value 0) from 10^3 (codded value-1), the rate of heat transfer is augmented about 300%. Again, when the value of Ra is raised to 10^6 (codded value 1) from 500,500 (codded value 0), the Nu_{av} is also increased about 18.3%. Additionally, Figure 8(b) illustrates a 3D surface view for observing the controls of Ra and Ha on Nu_{av}. The physical explanation of this occurrence is that as the magnitude of Ra grows, the natural convective propensity strengthens simultaneously. On the other hand, in Figures 9 and 10, due to the rise of Ha, the Nu_{av} reduces gradually. The physical enlightenment for this finding is that when an outer magnetic field is provided, a larger field interacts with stirring fluid, which reduces the flow circulation of the entire cavity. Furthermore, Figure 9 expresses another 2D and 3D graphical representations to represent the impact of Ra and ϕ on Nu_{av} for this hybrid nanofluid model. Also, the rate of Nu_{av} is boosted up due to the rise of Ra and ϕ, while Ha remains fixed. At the maximum value of Ra and ϕ (coded value 1), this changing rate of Nu_{av} is maximum, which is clear from the 2D contour Figure 9(a). Similarly, Figure 10 symbolizes the impact of Ha and ϕ on Nu_{av}. In this case, the changing rate of Nu_{av} is developed by raising the size of ϕ with diminishing the magnetic field (Ha). But this changing rate of Nu_{av} is smaller than the previous two cases.

4.6. Sensitivity Analysis. A crucial component of numerical simulation is sensitivity analysis, which is a tool for determining how uncertainty in a model's input influences the model's response. Performing a "sensitivity analysis" to determine how much the model's parameter affects the resultant variables is another

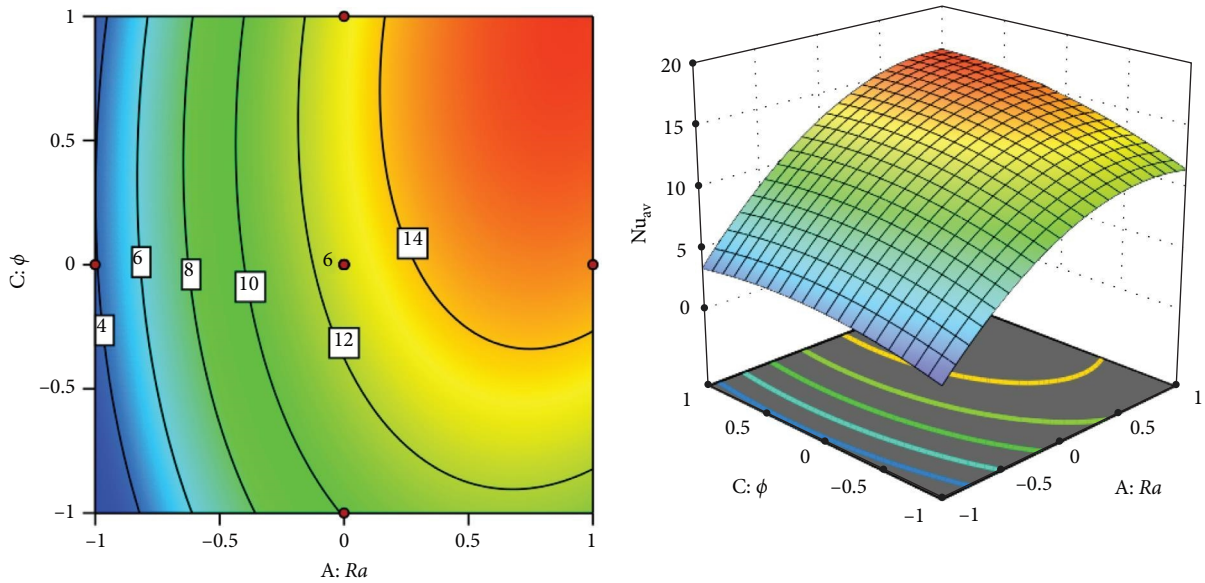

(a) (b)

FIGURE 9: Effect on Nu_{av} for Ra and ϕ: (a) 2D sight and (b) 3D sight.

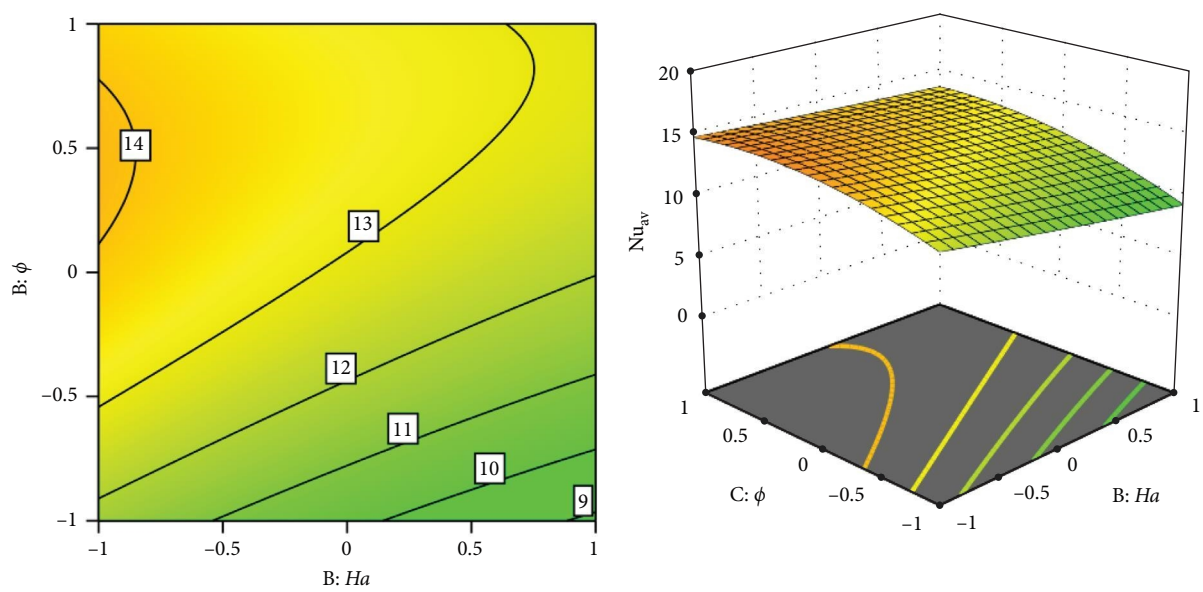

(a) (b)

FIGURE 10: Effect on Nu_{av} for Ha and ϕ: (a) 2D sight and (b) 3D sight.

definition of the term [53]. The most effective parameter can be found by ranking the significant parameters based on their influence using the findings of the sensitivity analysis. Mathematically, the partial derivatives of the response function concerning independent components are utilized to figure out the sensitivity of the yield function to efficient input elements (Ra, Ha, and ϕ). This results in an estimation of the response function Nu_{av}, which is Equation (13) to the input parameters as follows:

$$\frac{\partial Nu_{av}}{\partial Ra} = 5.41 - 6.86Ra - 0.9929Ha + 0.8413\phi, \tag{14}$$

$$\frac{\partial Nu_{av}}{\partial Ha} = -0.9061 - 0.9929Ra, \tag{15}$$

$$\frac{\partial Nu_{av}}{\partial \phi} = 1.50 - 2.32\phi + 0.8413Ra. \tag{16}$$

Table 9: Sensitivity analysis for Nu_{av}.

Ra	Ha	ϕ	$\frac{\partial Nu_{av}}{\partial Ra}$	$\frac{\partial Nu_{av}}{\partial Ha}$	$\frac{\partial Nu_{av}}{\partial \phi}$
0	0		5.41	−0.9061	1.50
	−1	0	6.4029	−0.9061	1.50
	1		4.4171	−0.9061	1.50
	0	−1	4.5687	−0.9061	3.82
1	−1	1	0.3842	−1.899	0.0231

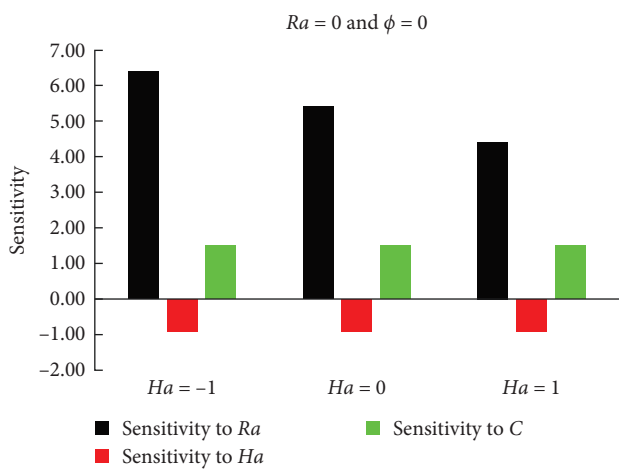

Figure 11: Sensitivity of response function (Nu_{av}) at $Ra = 0$ and $\phi = 0$.

Now, using Equations (14) and (16), we can determine the rate of sensitivity of the response function (Nu_{av}), and the outcomes are exhibited in Table 9. Here, to see the sensitivity rate the codded value of Ra is used 0 and 1; codded value of Ha is used at −1, 0, and 1; and the codded value of ϕ is taken as 0, −1, and 1. It is also important to remember that a positive sensitivity indicates that the input factors amplify the reaction. This demonstrates that the Ra and ϕ have a positive influence on the Nu_{av}. A negative sensitivity, on the other hand, demonstrates the polar opposite trend, where growing the input factors gives the reaction to go down. This shows that the input factor Ha has a detrimental impact on Nu_{av}. Furthermore, the straight bar in Figure 11 represents positive sensitivity to Nu_{av}, whereas the flipped bar represents negative sensitivity to Nu_{av}. The sensitivity grade is also shown by the overall length of the vertical bar.

5. Conclusion

In this work, heat transfer consequences based on natural convective hexagonal heat exchanger consuming hybrid ($Cu–TiO_2–H_2O$) nanofluid are investigated. Considering the relationship of heat transport mechanisms under the impact of the magnetic effect in particular. A numerical solution is built to encompass the complicated phenomena using the Galerkin infinite element method. The statistical methodology known as RSM is used to investigate the sensitivity study of the output function for an in-depth evaluation of the heat conveyance mechanism. The effect of hybrid nanofluid on streamlines, isotherms, and Nu_{av} is studied. Additionally, utilizing RSM, several 2D and 3D surface plots are provided for clear visualization of the heat transportation method with implicated critical components. A best fitted regression equation is also developed by statistical the RSM technique. Because of the exceptional thermal properties of the hybrid nanofluid, the $Cu–TiO_2–H_2O$ exceeds the heat transfer efficiency of the base fluid by 35.85%. Also, the $Cu–H_2O$ and $TiO_2–H_2O$ nanofluids express 34.3% and 29.38% greater heat transmission liken to base fluid, respectively. Furthermore, the Ha has an immediate negative impact on the velocity distribution of this hybrid nanofluid. Finally, the sensitivity analysis shows that the parameters Ra and ϕ have a favorable effect on Nu_{av}, but Ha has a negative effect on heat transmission from heated surfaces. By using RSM, the discussion about sensitivity analysis and explanation of the 3D surface plot, for natural convective hexagonal heat exchanger containing hybrid nanofluid, is the main novelty of this work.

Nomenclature

c_p: Specific heat at constant pressure ($J.kg^{-1}.K^{-1}$)
Nu: Nusselt number
k: Thermal conductivity ($W.m^{-1}.K^{-1}$)
g: Acceleration due to gravity ($m.s^{-1}$)
P: Pressure without dimension
Ra: Rayleigh number
Ha: Hartmann number
Pr: Prandtl number
U, V: Velocity component without dimension
u, v: Dimensional velocity component ($m.s^{-1}$)
X, Y: Dimensionless Cartesian coordinates
x, y: Dimensional Cartesian coordinates
H_2O: Water
Cu: Copper
TiO_2: Titanium dioxide
HS: Hot surface
L: Enclosure length (m)

Greek Symbols

α: Thermal diffusivity ($m^2.s^{-2}$)
ϕ: Nanoparticle volume fraction
β: Thermal expansion coefficient of (K^{-1})
ν: Kinematic viscosity ($m^2.s^{-1}$)
θ: Dimensionless temperature
ρ: Density ($kg.m^{-3}$)
μ: Dynamic viscosity ($kg.m^{-1}.s^{-1}$)
ψ: Stream function
Ω: Vorticity vector
σ: Electrical conductivity ($\Omega^{-1}.m^{-1}$)

Subscripts

av: Average
bf: Base fluid
sp: Solid particle
hnf: Hybrid nanofluid.

Abbreviations

2D: Two dimensional
3D: Three dimensional
FEM: Finite element method
RSM: Response surface methodology
MHD: Magnetohydrodynamics.

Data Availability

The study adopts a numerical technique, with no external data used in its findings.

Conflicts of Interest

The authors proclaim that they have no conflicts of interest.

References

[1] M. Saleem, M. A. Hossain, S. C. Saha, and Y. Gu, "Heat transfer analysis of viscous incompressible fluid by combined natural convection and radiation in an open cavity," *Mathematical Problems in Engineering*, vol. 2014, Article ID 412480, 14 pages, 2014.

[2] M. Sheikholeslami, "Modeling investigation for energy storage system including mixture of paraffin and ZnO nano-powders considering porous media," *Journal of Petroleum Science and Engineering*, vol. 219, Article ID 111066, 2022.

[3] H. Waqas, S. A. Khan, U. Farooq, T. Muhammad, A. Alshehri, and S. Yasmin, "Thermal transport analysis of six circular microchannel heat sink using nanofluid," *Scientific Reports*, vol. 12, Article ID 8035, 2022.

[4] S. M. Seyyedi, M. Hashemi-Tilehnoee, and M. Sharifpur, "Impact of fusion temperature on hydrothermal features of flow within an annulus loaded with nanoencapsulated phase change materials (NEPCMs) during natural convection process," *Mathematical Problems in Engineering*, vol. 2021, Article ID 4276894, 14 pages, 2021.

[5] M. J. Uddin, J. Al-Balushi, S. Mahatabuddin, and M. M. Rahman, "Convective heat transport for copper oxide–water nanofluid in an isosceles triangular cavity with a rippled base wall in the presence of magnetic field," *International Journal of Thermofluids*, vol. 16, Article ID 100195, 2022.

[6] M. Sheikholeslami, "Numerical analysis of solar energy storage within a double pipe utilizing nanoparticles for expedition of melting," *Solar Energy Materials and Solar Cells*, vol. 245, Article ID 111856, 2022.

[7] S. U. Choi and J. A. Eastman, *Enhancing Thermal Conductivity of Fluids with Nanoparticles (No. ANL/MSD/CP-84938; CONF-951135-29)*, Argonne National Lab.(ANL), Argonne, IL (United States), 1995.

[8] M. Sheikholeslami, R. Ellahi, and C. Fetecau, "CuO–water nanofluid magnetohydrodynamic natural convection inside a sinusoidal annulus in presence of melting heat transfer," *Mathematical Problems in Engineering*, vol. 2017, Article ID 5830279, 9 pages, 2017.

[9] M. Sheikholeslami, Z. Said, and M. Jafaryar, "Hydrothermal analysis for a parabolic solar unit with wavy absorber pipe and nanofluid," *Renewable Energy*, vol. 188, pp. 922–932, 2022.

[10] H. F. Öztop, A. Sakhrieh, E. Abu-Nada, and K. Al-Salem, "Mixed convection of MHD flow in nanofluid filled and partially heated wavy walled lid-driven enclosure," *International Communications in Heat and Mass Transfer*, vol. 86, pp. 42–51, 2017.

[11] M. Sheikholeslami, S. A. Shehzad, and R. Kumar, "Natural convection of Fe_3O_4-ethylene glycol nanouid under the impact of electric field in a porous enclosure," *Communications in Theoretical Physics*, vol. 69, no. 6, Article ID 667, 2018.

[12] T. Hayat, A. Aziz, and A. Alsaedi, "Analysis of entropy production and activation energy in hydromagnetic rotating flow of nanoliquid with velocity slip and convective conditions," *Journal of Thermal Analysis and Calorimetry*, vol. 146, pp. 2561–2576, 2021.

[13] S. Islam, T. Bairagi, T. Islam, B. M. J. Rana, S. K. Reza-E-Rabbi, and M. M. Rahman, "Heatline visualization in hydromagnetic natural convection flow inside a prismatic heat exchanger using nanofluid," *International Journal of Thermofluids*, vol. 16, Article ID 100248, 2022.

[14] T. Hayat, M. W. Ahmad, S. A. Khan, and A. Alsaedi, "Computational treatment of statistical declaration probable error for flow of nanomaterials with irreversibility," *Advances in Mechanical Engineering*, vol. 14, no. 1, 2022.

[15] M. M. Kaleem, M. I. Asjad, M. Usman, and M. Inc, "Effects of natural convection flow of fractional Maxwell hybrid nanofluid by finite difference method," *Waves in Random and Complex Media*, pp. 1–16, 2023.

[16] T. Tayebi and A. J. Chamkha, "Entropy generation analysis during MHD natural convection flow of hybrid nanofluid in a square cavity containing a corrugated conducting block," *International Journal of Numerical Methods for Heat & Fluid Flow*, vol. 30, no. 3, pp. 1115–1136, 2019.

[17] S. Rostami, S. Aghakhani, A. Hajatzadeh Pordanjani et al., "A review on the control parameters of natural convection in different shaped cavities with and without nanofluid," *Processes*, vol. 8, no. 9, Article ID 1011, 2020.

[18] R. Ellahi, A. Zeeshan, A. Waheed, N. Shehzad, and S. M. Sait, "Natural convection nanofluid flow with heat transfer analysis of carbon nanotubes–water nanofluid inside a vertical truncated wavy cone," *Mathematical Methods in the Applied Sciences*, vol. 46, no. 10, pp. 11303–11321, 2023.

[19] H. K. Park, M. Y. Ha, H. S. Yoon, Y. G. Park, and C. Son, "A numerical study on natural convection in an inclined square enclosure with a circular cylinder," *International Journal of Heat and Mass Transfer*, vol. 66, pp. 295–314, 2013.

[20] H. Waqas, S. A. Khan, S. Yasmin et al., "Galerkin finite element analysis for buoyancy driven *copper*-water nanofluid flow and heat transfer through fins enclosed inside a horizontal annulus: applications to thermal engineering," *Case Studies in Thermal Engineering*, vol. 40, Article ID 102540, 2022.

[21] N. C. Roy, "MHD natural convection of a hybrid nanofluid in an enclosure with multiple heat sources," *Alexandria Engineering Journal*, vol. 61, no. 2, pp. 1679–1694, 2022.

[22] M. Al-Maliki, K. Al-Farhany, and I. E. Sarris, "Heat transfer in an inclined rectangular cavity filled with hybrid nanofluid attached to a vertical heated wall integrated with PCM: an experimental study," *Symmetry*, vol. 14, no. 10, Article ID 2181, 2022.

[23] N. Alipour, B. Jafari, and K. Hosseinzadeh, "Optimization of wavy trapezoidal porous cavity containing mixture hybrid nanofluid (water/ethylene glycol Go–Al_2O_3) by response surface method," *Scientific Reports*, vol. 13, Article ID 1635, 2023.

[24] P. M. Patil and M. Kulkarni, "Analysis of MHD mixed convection in a Ag–TiO_2 hybrid nanofluid flow past a slender cylinder," *Chinese Journal of Physics*, vol. 73, pp. 406–419, 2021.

[25] M. S. Islam, S. Islam, and M.-N.-A.-A. Siddiki, "Numerical simulation with sensitivity analysis of MHD natural convection using Cu–TiO_2–H_2O hybrid nanofluids," *International Journal of Thermofluids*, vol. 20, Article ID 100509, 2023.

[26] A. Abderrahmane, N. A. A. Qasem, O. Younis et al., "MHD hybrid nanofluid mixed convection heat transfer and entropy generation in a 3-D triangular porous cavity with zigzag wall and rotating cylinder," *Mathematics*, vol. 10, no. 5, Article ID 769, 2022.

[27] A. J. Chamkha, I. V. Miroshnichenko, and M. A. Sheremet, "Numerical analysis of unsteady conjugate natural convection of hybrid water-based nanofluid in a semicircular cavity," *Journal of Thermal Science and Engineering Applications*, vol. 9, no. 4, Article ID 041004, 2017.

[28] H. T. Kadhim, A. Al-Manea, A. N. Al-Shamani, and T. Yusaf, "Numerical analysis of hybrid nanofluid natural convection in a wavy walled porous enclosure: local thermal non-equilibrium model," *International Journal of Thermofluids*, vol. 15, Article ID 100190, 2022.

[29] N. Biswas, N. K. Manna, A. J. Chamkha, and D. K. Mandal, "Effect of surface waviness on MHD thermo-gravitational convection of Cu–Al_2O_3–water hybrid nanofluid in a porous oblique enclosure," *Physica Scripta*, vol. 96, no. 10, Article ID 105002, 2021.

[30] A. M. Rashad, A. J. Chamkha, M. A. Ismael, and T. Salah, "Magnetohydrodynamics natural convection in a triangular cavity filled with a Cu–Al_2O_3/water hybrid nanofluid with localized heating from below and internal heat generation," *Journal of Heat and Mass Transfer*, vol. 140, no. 7, Article ID 072502, 2018.

[31] B. Takabi and S. Salehi, "Augmentation of the heat transfer performance of a sinusoidal corrugated enclosure by employing hybrid nanofluid," *Advances in Mechanical Engineering*, vol. 6, Article ID 147059, 2014.

[32] S. S. U. Devi and S. P. A. Devi, "Numerical investigation of three-dimensional hybrid Cu–Al_2O_3/water nanofluid flow over a stretching sheet with effecting Lorentz force subject to Newtonian heating," *Canadian Journal of Physics*, vol. 94, no. 5, pp. 490–496, 2016.

[33] M. Sheikholeslami, I. Hashim, and S. Soleimani, "Numerical investigation of the effect of magnetic field on natural convection in a curved-shape enclosure," *Mathematical Problems in Engineering*, vol. 2013, Article ID 821725, 10 pages, 2013.

[34] K. Hosseinzadeh, M. A. E. Moghaddam, S. Nateghi, M. B. Shafii, and D. D. Ganji, "Radiation and convection heat transfer optimization with MHD analysis of a hybrid nanofluid within a wavy porous enclosure," *Journal of Magnetism and Magnetic Materials*, vol. 566, Article ID 170328, 2023.

[35] F. Selimefendigil and H. F. Öztop, "Corrugated conductive partition effects on MHD free convection of CNT-water nanofluid in a cavity," *International Journal of Heat and Mass Transfer*, vol. 129, pp. 265–277, 2019.

[36] T. Tayebi, H. F. Öztop, and A. J. Chamkha, "MHD natural convection of a CNT-based nanofluid-filled annular circular enclosure with inner heat-generating solid cylinder," *The European Physical Journal Plus*, vol. 136, Article ID 150, 2021.

[37] I. Chabani, F. Mebarek-Oudina, H. Vaidya, and A. I. Ismail, "Numerical analysis of magnetic hybrid Nano-fluid natural convective flow in an adjusted porous trapezoidal enclosure," *Journal of Magnetism and Magnetic Materials*, vol. 564, Part 2, Article ID 170142, 2022.

[38] M. Sheikholeslami, T. Hayat, and A. Alsaedi, "MHD free convection of Al_2O_3–water nanofluid considering thermal radiation: a numerical study," *International Journal of Heat and Mass Transfer*, vol. 96, pp. 513–524, 2016.

[39] O. Prakash, P. Barman, P. S. Rao, and R. P. Sharma, "MHD free convection in a partially open wavy porous cavity filled with nanofluid," *Numerical Heat Transfer, Part A: Applications*, vol. 84, no. 5, pp. 449–463, 2023.

[40] A. Mourad, A. Aissa, A. M. Abed et al., "MHD natural convection of Fe_3O_4–MWCNT/Water hybrid nanofluid filled in a porous annulus between a circular cylinder and Koch snowflake," *Alexandria Engineering Journal*, vol. 65, pp. 367–382, 2023.

[41] R. Mahesh, U. S. Mahabaleshwar, P. N. V. Kumar, H. F. Öztop, and N. Abu-Hamdeh, "Impact of radiation on the MHD couple stress hybrid nanofluid flow over a porous sheet with viscous dissipation," *Results in Engineering*, vol. 17, Article ID 100905, 2023.

[42] S. E. Ahmed, A. Mahdy, and M. A. Mansour, "Cattaneo–Christov heat flux impacts on MHD radiative natural convection of Al_2O_3–Cu–H_2O hybrid nanofluid in wavy porous containers using LTNE," *Nonlinear Analysis: Modelling and Control*, vol. 28, no. 3, pp. 431–446, 2023.

[43] J. Fereidooni, "Baffles' size impact on the heat transfer and second law features of magnetic hybrid nanofluid within a hexagonal-shaped porous domain," *Journal of Magnetism and Magnetic Materials*, vol. 582, Article ID 171037, 2023.

[44] A. M. Aly, A. Al-Hanaya, and Z. Raizah, "The magnetic power on natural convection of NEPCM suspended in a porous annulus between a hexagonal-shaped cavity and dual curves," *Case Studies in Thermal Engineering*, vol. 28, Article ID 101354, 2021.

[45] Z. Raizah and A. M. Aly, "Effect of dual-rotation on MHD natural convection of NEPCM in a hexagonal-shaped cavity based on time-fractional ISPH method," *Scientific Reports*, vol. 11, Article ID 22687, 2021.

[46] N. Faraz, M. Shemyal Nisar, Y. Khan, A. Hussain, and K. Iqbal, "Natural convection of Cu–H_2O nanofluid inside hexagonal enclosure fitted with a square cavity with a non-uniformly heated wall (s)," *Results in Physics*, vol. 51, Article ID 106648, 2023.

[47] F. Garoosi, F. Hoseininejad, and M. M. Rashidi, "Numerical study of heat transfer performance of nanofluids in a heat exchanger," *Applied Thermal Engineering*, vol. 105, pp. 436–455, 2016.

[48] M. Goodarzi, A. D'Orazio, A. Keshavarzi, S. Mousavi, and A. Karimipour, "Develop the nano scale method of lattice Boltzmann to predict the fluid flow and heat transfer of air in the inclined lid driven cavity with a large heat source inside, two case studies: pure natural convection & mixed convection," *Physica A: Statistical Mechanics and its Applications*, vol. 509, pp. 210–233, 2018.

[49] R. D. Plant and M. Z. Saghir, "Numerical and experimental investigation of high concentration aqueous alumina nanofluids in a two and three channel heat exchanger," *International Journal of Thermofluids*, vol. 9, Article ID 100055, 2021.

[50] T. Basak, S. Roy, and C. Thirumalesha, "Finite element analysis of natural convection in a triangular enclosure: effects of various thermal boundary conditions," *Chemical Engineering Science*, vol. 62, no. 9, pp. 2623–2640, 2007.

[51] D. C. Montgomery, *Design and Analysis of Experiments*, John Wiley & sons, 2017.

[52] G. E. Box and K. B. Wilson, "On the experimental attainment of optimum conditions," "Breakthroughs in Statistics: Methodology and Distribution," Springer, New York, NY, pp. 270–310, 1992.

[53] F. Campolongo and R. Braddock, "The use of graph theory in the sensitivity analysis of the model output: a second order screening method," *Reliability Engineering & System Safety*, vol. 64, no. 1, pp. 1–12, 1999.